AIP Advances

Magnetization dynamics in ordered spin structures revealed by diffractive and reflectometry ferromagnetic resonance

Cite as: AIP Advances **11**, 015327 (2021); https://doi.org/10.1063/9.0000058
Submitted: 15 October 2020 . Accepted: 20 November 2020 . Published Online: 11 January 2021

D. M. Burn, S. L. Zhang, G. van der Laan, and T. Hesjedal

Magnetization dynamics in ordered spin structures revealed by diffractive and reflectometry ferromagnetic resonance

Cite as: AIP Advances 11, 015327 (2021); doi: 10.1063/9.0000058
Presented: 3 November 2020 • Submitted: 15 October 2020 •
Accepted: 20 November 2020 • Published Online: 11 January 2021

D. M. Burn,[1,a)] S. L. Zhang,[2,3] G. van der Laan,[1] and T. Hesjedal[2]

AFFILIATIONS

[1] Diamond Light Source, Harwell Science and Innovation Campus, Didcot, Oxfordshire OX11 0DE, United Kingdom
[2] Clarendon Laboratory, Department of Physics, University of Oxford, Oxford OX1 3PU, United Kingdom
[3] School of Physical Science and Technology, ShanghaiTech University, Shanghai 200031, China

Note: This paper was presented at the 65th Annual Conference on Magnetism and Magnetic Materials.
[a)] **Author to whom correspondence should be addressed:** david.burn@diamond.ac.uk

ABSTRACT

Synchrotron radiation based techniques provide unique insight into both the element and time resolved magnetization behavior in magnetic spin systems. Here, we highlight the power of two recent developments, utilizing x-ray scattering techniques to reveal the precessional magnetization dynamics of ordered spin structures in the GHz regime, both in diffraction and reflection configurations. Our recently developed diffraction and reflectometry ferromagnetic resonance (DFMR and RFMR) techniques provide novel ways to explore the dynamics of modern magnetic materials, thereby opening up new pathways for the development of spintronic devices. In this paper we provide an overview of these techniques, and discuss the new understanding they provide into the magnetization dynamics in the chiral magnetic structure in Y-type hexaferrite and the depth dependence to the magnetization dynamics in a $[CoFeB/MgO/Ta]_4$ multilayer.

I. INTRODUCTION

Magnetic materials have played a pivotal role in the striking increase in performance of computer technologies over the past decades, most notably through the discovery of giant magnetoresistance and the subsequent improvements in hard disk storage density.[1] For the development of novel technologies, spintronics is a strong contender and the high-speed dynamic properties of magnetic materials are particularly important.

Various techniques are available for the measurement of the dynamic properties of magnetic materials including Brillouin-light scattering[2,3] and time-resolved magneto-optical Kerr effect measurements.[4] Typically, broadband or cavity ferromagnetic resonance (FMR) is used to measure the power absorbed by a material when an RF magnetic field is applied to excite the dynamics in the spin system.[5,6] Mapping out the power absorption as a function of RF frequency and applied bias magnetic field provides insight into the dynamic modes being excited within the magnetic material. The orientation of the magnetization during ferromagnetic resonance can be described by the time evolution of precessional damping terms. Their combined action results in the magnetization mapping out a cone about the effective magnetic field axis.

Recently, more complex magnetically ordered materials have become the focus of much attention as they are promising for high-density and low-energy consumption devices.[7] These systems exhibit chiral magnetic phases such as helical, conical or skyrmion spin structures resulting from the Dzyaloshinskii–Moriya interaction (DMI)[8,9] found in noncentrosymmetric bulk materials[10,11] and in systems where symmetry breaking occurs at a ferromagnetic/heavy metal interface.[12] These spin structures are much more complex than simple ferromagnetic structures, and so is their dynamic behavior.

Until recently, our understanding of magnetization dynamics in ordered magnetic materials was based on techniques which probe the sample-averaged FMR response which is analyzed

alongside simulated micromagnetic behavior.[13] Here, we highlight the power of synchrotron-based characterization techniques for probing magnetization dynamics of both chiral magnetic structures and artificially engineered magnetic multilayers.

The new advances in synchrotron-based techniques are built on the well-established x-ray magnetic circular dichroism (XMCD) effect, which provides element-specific sensitivity to the magnetization orientation by using circularly polarized x-rays at an absorption edge of a specific magnetic species.[14–16] Coupled with the pulsed nature of synchrotron x-ray sources, stroboscopic measurements with the magnetization excited at resonance at an RF frequency which is a multiple of the synchrotron bunch frequency provides a mechanism to explore element specific magnetization dynamics. The combination of XMCD and FMR is known as x-ray detected ferromagnetic resonance (XFMR) and has been adopted and developed at various synchrotrons.[17–20] XFMR has given significant insight into the element specific magnetization dynamics in magnetically coupled bi- and trilayer systems, for example in spin valves and magnetic tunnel junctions.[21,22]

In magnetically ordered systems, x-rays can probe the periodic structure of materials, making use of interference effects from x-rays scattered from the regularly repeating magnetization density variations within a structure. This scattering leads to pure magnetic x-ray scattering peaks which reveal information about the static magnetic structure. Analysis of these magnetic peaks in resonant elastic x-ray scattering (REXS) measurements has led to significant progress in the understanding of chiral magnetic systems.[23]

In chiral systems, the magnetic ordering occurs due to the DMI interaction imposing a physical repetition of the magnetic structure. In magnetic multilayer systems, magnetic ordering is also achieved through the artificially induced structure resulting from the growth of the different layers. In these systems, analysis of the specular reflectivity can provide detailed insight into the depth profile of the magnetic structure of the system.[24,25]

Measurements of the magnetization dynamics of magnetically ordered systems have recently been demonstrated by applying XFMR detection techniques in both diffraction and reflectometry geometries, i.e., DFMR[26] and RFMR,[27] respectively. In this paper, we discuss the unique power of these novel experimental techniques. We highlight some of the first results which reveal the complex dynamic behavior coupled to the chiral spin structure in Y-type hexaferrite $Ba_2Mg_2Fe_{12}O_{22}$.[26] We also show how the magnetization dynamics in a $[CoFeB/MgO/Ta]_4$ multilayer has been revealed as a function of depth.[27]

In Sec. II we will first describe what is common between the DFMR and RFMR techniques, before discussing the specific application of each technique to our example systems. In Sec. III, results measured from the two example systems are discussed in turn and a comparison of the two technique, with their merits, is drawn up in Sec. IV.

II. EXPERIMENTAL

Our experiments, which probe the magnetization dynamics through detection of scattered x-rays, make use of several of the unique properties of synchrotron radiation. We will discuss here our experiments performed in the RASOR soft x-ray diffractometer on beamline I10 at the Diamond Light Source.[28] Our experimental setup is illustrated schematically in Fig. 1. Incident x-rays with wavevector k_i illuminate the sample and the scattered beam (k_s) is detected using a photodiode. The geometry of the diffractometer is configured to probe the system at certain diffraction or specular reflectivity conditions.

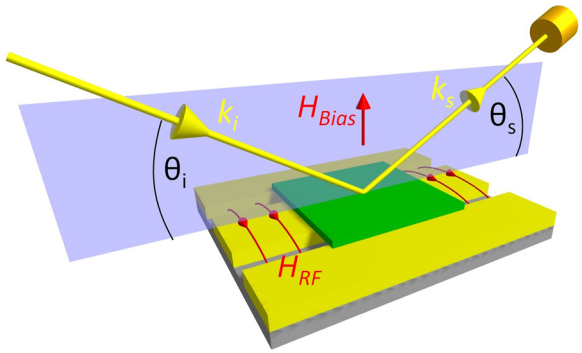

FIG. 1. Schematic showing a magnetic sample mounted on top of a coplanar waveguide which provides an RF magnetic field, H_{RF}. An additional bias field, H_{Bias}, is applied by permanent magnets with an adjustable gap and field direction in the scattering plane. Incident polarized x-rays (k_i) probe the sample, and the scattered beam (k_s) is measured with a photodiode detector. Figure adapted from Burn *et al.*, Nano Lett. **20**, 345 (2020). Copyright 2020 Authors, licensed under a Creative Commons Attribution CC BY 4.0.

The sample is mounted on a coplanar waveguide (CPW) which in turn is mounted on the end of a liquid He cryostat arm. Sample temperatures down to 12 K can be reached in external fields up to 200 mT. The field is supplied by two permanent magnets which can be positioned to vary the field strength and orientation within the scattering plane.

In addition to the applied bias field, passing an RF current through the CPW generates a transverse RF magnetic field around the central conductor of the waveguide. With the sample positioned in close proximity above the surface of the waveguide, the RF field is used to excite the magnetization dynamics in the system. Note, that in contrast to conventional XFMR measurements where the sample is mounted flip-chip onto the CPW, in the scattering geometry the sample is mounted face up to allow for the x-ray beam to probe its surface. Therefore, to ensure good coupling between the CPW and the surface that is probed on top of the sample, the sample must either be thinned, or in the case of multilayers, grown on a thin substrate of the order of 100 μm.

In the experiment, the photon energy of the incident x-rays is first tuned to the atomic absorption edge to be probed; in both the hexaferrite and multilayer examples this is the Fe L_3 absorption edge at ~707 eV. This energy is verified by measuring the fluorescence yield from the sample as a function of photon energy away from any reflection or diffraction condition. The fluorescence yield provides a measure of the absorption edge energy without the additional scattering effects which affect the reflected and diffracted beams. The energy at which the maximum contrast from the x-ray magnetic circular dichroism (XMCD) is obtained coincides with that of the absorption edge.

With the x-ray beam tuned to the energy of interest, the static nature of the scattering from the sample is now characterized. The location and intensity of the scattered peaks or reflected beam is found in reciprocal space based on the energy of the incident beam and the incident and scattered beam directions from the sample. This is done using a photodiode detector to which slits are added to reduce the angular acceptance of the detector, thereby increasing the angular resolution. In diffraction, both structural and magnetic scattering peaks are first identified, followed by the exploration of the magnetic peak intensity as a function of the applied magnetic field.

Once the detector is aligned to one of the magnetic scattering peaks, the stroboscopic XFMR detection scheme is used to probe the dynamics of the ordered magnetic structure that gives rise to that scattering peak. A RF magnetic field is applied to the sample with a frequency at (*i*) an integer multiple of the synchrotron master clock, ~500 MHz, and (*ii*) at a crossing of the ferromagnetic resonance mode, tuned by the external static bias field, H_{Bias}. For this purpose, the frequency-field dependence to the ferromagnetic resonance modes are typically precharacterized through offline vector-network-analyzer (VNA) FMR measurements.

The synchronization between the RF field and the synchrotron clock allows snapshots of the magnetization dynamics to be probed stroboscopically with the synchrotron x-ray bunches. The pulse width of the bunches is 20-30 ps, while the jitter in the synchronization is below 10 ps.[29]

To improve the signal-to-noise ratio of the dynamic signal, additional lock-in techniques are used. Here, the phase of the RF field is modulated by 180° at a frequency of ~2 kHz. This frequency is chosen to be just below the bandwidth of the photodiode. The modulation is achieved by switching between two delay lines where the difference in length corresponds to a electronic signal phase delay of 180° for the RF frequency used. The 180° phase modulation gives an advantage over traditional chopping of the signal (amplitude modulation) in that the measured signal is doubled in size and that the RF power load on the sample remains constant.

An additional variable length delay line is used to vary the delay between the RF excitation (pump) and x-ray bunch (probe). This allows the time evolution of the magnetization precession to be mapped out. The dynamic signal is stroboscopically measured for a range of delays covering 1-2 periods of the excitation waveform. The dynamic intensity as a function of delay is measured over a range of magnetic fields. When crossing over the ferromagnetic resonance mode, fitting of the sinusoidal delay signal typically reveals a Lorentzian peak shape in amplitude, accompanied by a 180° shift in phase.

In Y-type hexaferrite, the chiral magnetic ordering results in x-ray scattering and the manifestation of diffraction peaks relating to both the charge and magnetic structure. For this sample, the stroboscopic dynamic measurements are performed in a diffractive ferromagnetic resonance (DFMR) experiment. The resonance dynamics is probed as a function of the magnetic field and the incident x-ray polarization. We also consider the scattering effects within a magnetic multilayered system, in which a reflectometry signal provides information on the depth profile of both the chemical and magnetic through the system.[30] Here, the stroboscopic dynamic technique is measured as a function of Q_z, the momentum transfer through the depth of the sample. The reflectometry ferromagnetic resonance (RFMR) technique provides insight into the depth dependence of the dynamic magnetization behavior through the multilayer system.

III. RESULTS

A. DFMR on Y-type hexaferrite

First we consider the DFMR experiment on the Y-type hexaferrite system. Initially the static magnetic scattering pattern of the sample was obtained. These static results allow for the precise tuning of the energy to the Fe L_3 absorption edge, confirming the origin of the magnetic contrast via XMCD. The hexaferrite is a rich magnetic systems, showing, e.g., antiferromagnetic order and chiral magnetic structures.[31–33] First, the diffraction peaks arising from the periodic magnetic structures are identified. The photodiode detector was then aligned to the scattering peak representing the conical modulation of the magnetization. With an RF excitation field applied to the sample, the stroboscopic detection scheme was used to measure the dynamic contribution to the scattered intensity on this peak as snapshots covering the dynamic precession.

Figure 2(a) shows this dynamic contribution to the intensity and its variation as a function of the delay between the RF pump and x-ray probe. The signal shows a sinusoidal variation with a period of 166 ps corresponding to the 6 GHz frequency used to excite the magnetization dynamics. The sinusoidal nature of this signal results from the change in projection of the magnetization relative to the incident and scattered beam directions as the magnetization precesses. The amplitude and phase of the dynamic signal were extracted from sinusoidal fits to the delay scan data in Fig. 2(a), and are plotted as a function of magnetic field in Figs. 2(b) and 2(c), respectively. The amplitude fits well to a Lorentzian peak shape with a corresponding 180° shift in the phase coinciding with the center of the peak. These features are indicative of the crossing of a FMR mode, which at 6 GHz occurs at 52 mT with a full width half maximum of 13 mT.

Since this resonance in Fig. 2 is measured on the chiral magnetic scattering peak, the magnetization dynamics must be coupled to the chiral magnetic phase in this material. Further understanding about the magnetization dynamics of the resonance mode stemming from the chiral ordering can be obtained by probing the system with linearly polarized light at different polarization angles. This is achieved by sitting at the optimum resonance conditions (6 GHz, 52 mT) and measuring the intensity of the stroboscopically detected scattered beam as a function of the angle of the linearly polarized incident x-rays.

Figure 3 shows the dynamic contribution to the scattered peak intensity as a function of both the linear polarization angle η and the delay. The polarization is measured with respect to vertically polarized x-rays at an angle of $\eta = 0°$. Similarly to the delay scans in Fig. 2(a), Fig. 3 shows sinusoidal variations in the dynamic signal as a function of the delay with a 166 ps period corresponding to the 6 GHz excitation frequency. The amplitude of this sinusoidal signal is governed by an additional modulation as a function of η whereby the amplitude of the signal is strong at $\eta = 45°$ and 135°, whilst at $\eta = 90°$ and 180° this amplitude is negligible. This modulation of the amplitude shows a $\eta = 180°$ repetition cycle resulting from the orientation of the linear polarization of the light when

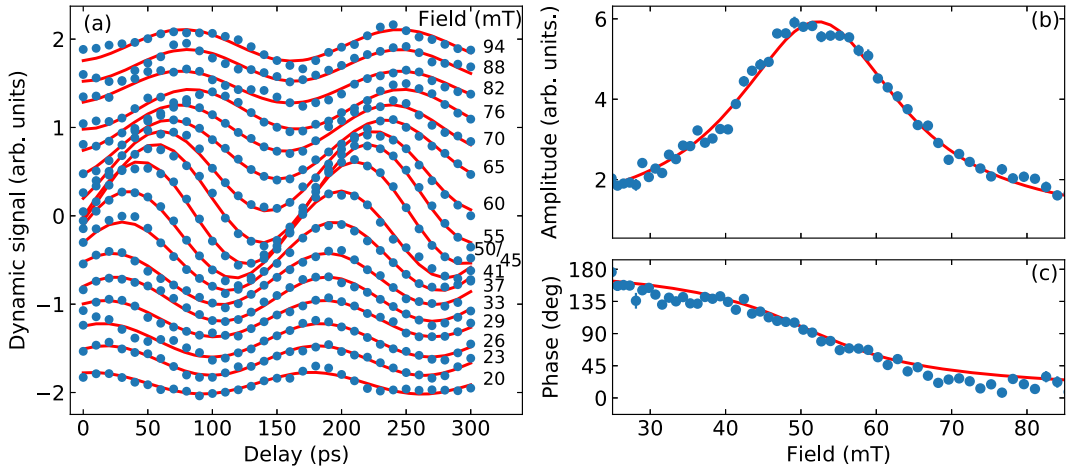

FIG. 2. (a) Dynamic contribution to the scattered peak intensity as a function of pump-probe delay measured at various fields (offset for clarity) at the Fe L_3 edge with circularly polarized x-rays. Sinusoidal fits reveal the variation in (b) the amplitude and (c) phase as a function of magnetic bias field revealing a resonance peak in the amplitude accompanied by a 180° shift in phase. The lines in (b) and (c) show a Lorentzian fit and arctan transition across the resonance. Figure adapted from Burn *et al.*, Nano Lett. **20**, 345 (2020). Copyright 2020 Authors, licensed under a Creative Commons Attribution CC BY 4.0.

rotated about the propagation direction of the beam. The phase of the dynamic signal remains independent of η and there are negligible differences between measurements on either of the two chiral magnetic satellites.

Soft x-ray scattering of linearly polarized x-rays tuned to a resonance is sensitive to the periodic structure of all three components of the magnetization orientation within the system. The scattered intensity can be calculated by considering structural as well as magnetic scattering effects, and their mutual interference. For the case of a fixed scattering geometry on a magnetic peak, the intensity variations as a function of polarization angle represent changes in the 3-dimensional magnetic structure. In the dynamic regime, varying the polarization angle therefore reveals a signal containing further insight into the time-dependence of the magnetization orientation during precession.

In a field-polarized ferromagnetic system, the dynamic behavior can be understood as a time-dependent modulation of the uniformly aligned static magnetization configuration about a conical precessional shape. In the non-colinear chiral static spin structure, following a similar approach, the introduction of a conical modulation of the spins about their static structure provides a first approximation of the dynamic behavior. Comparison between the experimental results and simulations of the expected time-dependent scattering provide allow further insight into the modal dynamics of the system to be extracted.[26]

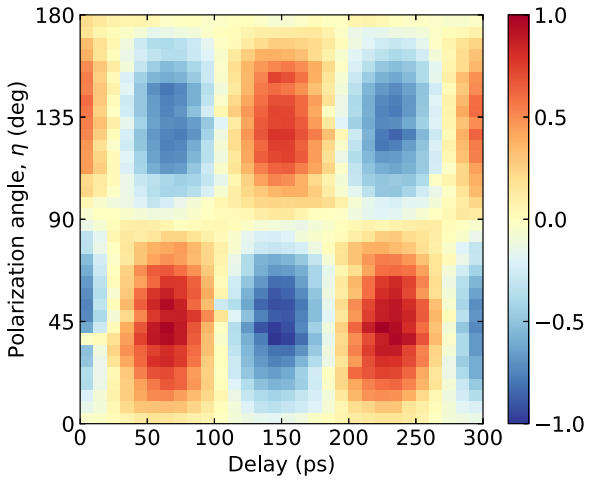

FIG. 3. Dynamic contribution to the scattered intensity at one of the chiral magnetic scattering peaks in Y-type hexaferrite as a function of both linear polarization angle, η, and delay. The measurement was carried out at the Fe L_3 edge in a field of 52 mT. Figure adapted from Burn *et al.*, Nano Lett. **20**, 345 (2020) with permission from the authors. Copyright 2020 Authors, licensed under a Creative Commons Attribution CC BY 4.0.

B. RFMR on a [CoFeB/MgO/Ta]$_4$ multilayer

In the $[CoFeB/MgO/Ta]_4$ multilayer system, the depth profile of the system is characterized through x-ray reflectometry and the depth dependence to the magnetization dynamics is revealed through a RFMR experiment. The differences in electron density between the layers give rise to abrupt changes in the optical properties through the material. Static soft x-ray reflectivity analysis, with the x-ray energy again tuned to the absorption edge of the element of interest, is first performed on the samples allowing the structure of the film to be determined through fitting techniques. This confirms the layered structure of the material and also the location of the magnetic species within the depth profile of the structure.

When measured stroboscopically in the dynamic regime, a sinusoidal variation in the reflected signal is observed similar to that seen in Fig. 2(a). Again, by fitting the sinusoidal delay scans, the

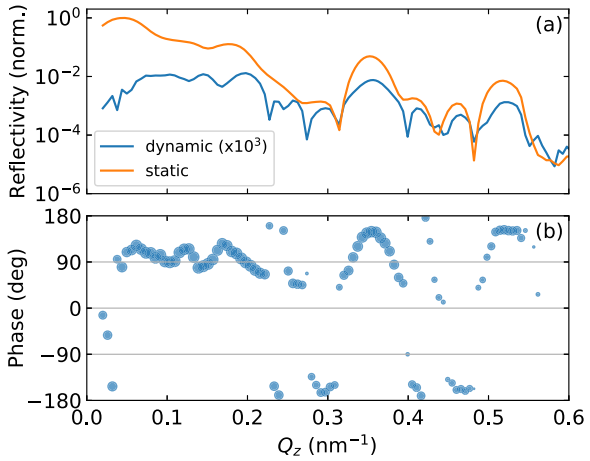

FIG. 4. Reflectivity from a $[CoFeB/MgO/Ta]_4$ multilayer as a function of Q_z, measured at the Fe L_3 edge in an out-of-plane field of 29 mT. (a) Static contribution and the amplitude of the dynamic contribution to the reflectivity, and (b) phase of the dynamic contribution. Figure adapted from Burn *et al.*, Phys. Rev. Lett. **125**, 137201 (2020) with permission from the authors. Copyright 2020 Authors, licensed under a Creative Commons Attribution CC BY 4.0.

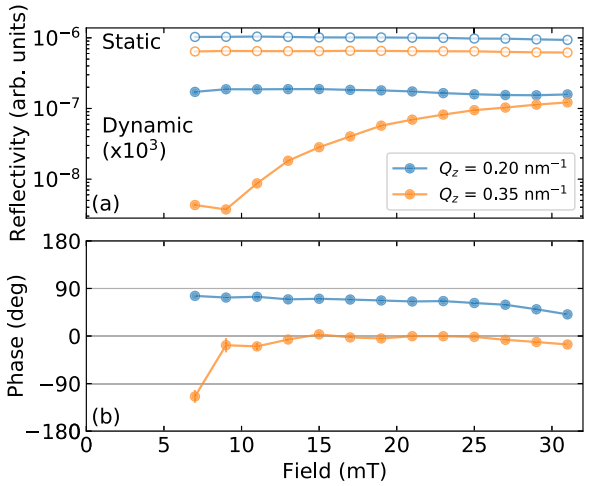

FIG. 5. (a) Static response and amplitude of the dynamic contribution to the reflected intensity, and (b) phase of the dynamic contribution as a function of out-of-plane bias field. The measurement on $[CoFeB/MgO/Ta]_4$ was carried out at the Fe L_3 edge with circularly polarized x-rays for two different Q_z values.

amplitude and phase of the dynamic signal are extracted and Fig. 4 shows these quantities plotted alongside the static reflectivity as a function of Q_z.

The static intensity, and the amplitude of the dynamic signal in Fig. 4(a), show reflectivity fringes resulting from interference effects due to both the layered chemical and magnetic structure of the sample. In the dynamic case, additional minima are also observed. The phase of the dynamic signal in Fig. 4(b) shows variations with two contributions. Firstly, abrupt 180° jumps in the phase occur, coinciding with minima in the amplitude of the dynamic signal. Secondly, there are additional, smoother variations in the phase. The 180° jumps in phase correspond to inversion of the sign of the XMCD signal measured at different scattering conditions, whilst the smoother variations in the phase have been attributed to variations in the magnetization dynamics occurring between the magnetic layers in the multilayered structure.

The magnetic resonance behavior in the system can be manipulated by adjusting the applied magnetic field. In Fig. 2 the crossing of a ferromagnetic resonance was demonstrated. In the multilayer system, selected Q_z points were monitored as a function of the magnetic field ranging from 7 to 31 mT, and both the static and dynamic contributions to the reflectivity are shown in Fig. 5. Firstly, at both Q_z values, there is negligible effect of the magnetic field on the static intensity. The dynamic signal varies in amplitude as a function of field for Q_z = 0.35 nm^{-1}, on the magnetic superlattice peak, but not at 0.20 nm^{-1}. This shows that even though the static magnetic structure of the film is not affected by field changes in this range, the magnetization dynamics are.

The phase of the signal in Fig. 5(b) shows a gradual reduction for Q_z = 0.20 nm^{-1} despite a negligible change in the amplitude. The inverse occurs at Q_z = 0.35 nm^{-1} where the change in phase is negligible despite a significant change in amplitude.

IV. DISCUSSION

In XFMR measurements, detection of the luminescence from the substrate traditionally provides a measure of the x-ray absorption, however, this also imposes the limitation that a luminescent substrate is required.[21] Layer dependent dynamics can be extracted if the layers contain at least one unique element, e.g., by measuring at the Ni and Co edge in a NiFe/CoFe bilayer.

In RFMR measurements, the depth-dependent and therefore layer specific insight originates from scattering effects, i.e., neither the chemical makeup of the layers nor the number of layers are any longer a constraint. Furthermore, the reflected x-ray beam is detected with no need for a luminescent substrate. RFMR measurements require the scattering plane to be unobstructed, which limits the applicable magnetic field range. Further, for good coupling of the RF field to the film which is now facing away from the coplanar waveguide, thin (or thinned down) substrates are required.

Similarly to RFMR, DFMR requires the scattering plane to be clear of obstacles and the coupling of the RF field to the sample to be increased through substrate thinning. The main advantage with DFMR is that it can probe the dynamics coupled to ordered magnetic systems with a propagation direction along any axis within the sample. This is only limited by the requirement to fulfill the diffraction condition which is constrained by the geometry of the diffractometer and the wavelength of the x-rays. For RFMR a diffraction peak is not required, or in fact either the need for any crystalline order.

V. CONCLUSIONS

In conclusion, we have discussed the combination of soft x-ray based synchrotron techniques with FMR to probe the magnetization dynamics in ordered magnetic systems. XMCD provides dichroic

contrast to the magnetization orientation, and when measured stroboscopically with the x-ray pulses synchronized to an applied RF field, XFMR provides a measure of the time evolution of the magnetization orientation during dynamic precession. Soft x-ray diffraction and reflectometry techniques based on x-ray scattering are ideal tools to probe ordered magnetic systems and the stroboscopic measurement of a reflected or diffracted signal allows the magnetization dynamics of ordered magnetic systems to be investigated. We have demonstrated the capabilities of RFMR and DFMR through the exploration of Y-type hexaferrite and $[CoFeB/MgO/Ta]_4$ multilayers, giving new insights into their previously hidden dynamics. Our characterization tools for the exploration of the dynamics of chiral and multilayered magnetic materials are significant to the development of high-density and low-energy consumption data processing solutions.

ACKNOWLEDGMENTS

We aknowledge Diamond Light Source for beamtime on I10 under proposal numbers SI18898 and MM23895.

DATA AVAILABILITY

Raw data were generated at the Diamond Light Source large scale facility. Derived data supporting the findings of this study are available from the corresponding author upon reasonable request.

REFERENCES

[1] S. Parkin, X. Jiang, C. Kaiser, A. Panchula, K. Roche, and M. Samant, Proc. IEEE **91**, 661 (2003).
[2] S. Demokritov and E. Tsymbal, J. Phys. Condens. Matter **6**, 7145 (1994).
[3] S. O. Demokritov, B. Hillebrands, and A. N. Slavin, Phys. Rep. **348**, 441 (2001).
[4] M. R. Freeman, R. R. Ruf, and R. J. Gambino, IEEE Trans. Magn. **27**, 4840 (1991).
[5] J. H. E. Griffiths, Nature **158**, 670 (1946).
[6] C. Kittel, Phys. Rev. **73**, 155 (1948).
[7] X. Z. Yu, N. Kanazawa, W. Z. Zhang, T. Nagai, T. Hara, K. Kimoto, Y. Matsui, Y. Onose, and Y. Tokura, Nat. Commun. **3**, 988 (2012).
[8] I. Dzyaloshinksy, J. Phys. Chem. Solids **4**, 241 (1958).
[9] T. Moriya, Phys. Rev. **120**, 91 (1960).
[10] W. Münzer, A. Neubauer, T. Adams, S. Mühlbauer, C. Franz, F. Jonietz, R. Georgii, P. Böni, B. Pedersen, M. Schmidt, A. Rosch, and C. Pfleiderer, Phys. Rev. B - Condens. Matter Mater. Phys. **81**, 041203 (2010).
[11] S. Mühlbauer, Science **323**, 915 (2011).
[12] M. Bode, M. Heide, K. Von Bergmann, P. Ferriani, S. Heinze, G. Bihlmayer, A. Kubetzka, O. Pietzsch, S. Blügel, and R. Wiesendanger, Nature **447**, 190 (2007).
[13] M. Garst, J. Waizner, and D. Grundler, J. Phys. D. Appl. Phys. **50**, 293002 (2017).
[14] G. van der Laan, B. T. Thole, G. A. Sawatzky, J. B. Goedkoop, J. C. Fuggle, J.-M. Esteva, R. Karnatak, J. P. Remeika, and H. A. Dabkowska, Phys. Rev. B **34**, 6529 (1986).
[15] G. Schütz, W. Wagner, W. Wilhelm, P. Kienle, R. Zeller, R. Frahm, and G. Materlik, Phys. Rev. Lett. **58**, 737 (1987).
[16] G. van der Laan and A. I. Figueroa, Coord. Chem. Rev. **277-278**, 95 (2014).
[17] C. Klewe, Q. Li, M. Yang, A. T. N'Diaye, D. M. Burn, T. Hesjedal, A. I. Figueroa, C. Hwang, J. Li, R. J. Hicken, P. Shafer, E. Arenholz, G. van der Laan, and Z. Qiu, Synchrotron Radiat. News **33**, 12 (2020).
[18] J. Goulon, A. Rogalev, F. Wilhelm, G. Goujon, C. Brouder, A. Yaresko, J. Ben Youssef, and M. V. Indenbom, J. Magn. Magn. Mater. **322**, 2308 (2010).
[19] K. Ollefs, R. Meckenstock, D. Spoddig, F. M. Römer, C. Hassel, C. Schöppner, V. Ney, M. Farle, and A. Ney, J. Appl. Phys. **117**, 223906 (2015).
[20] H. G. Bauer, P. Majchrak, T. Kachel, C. H. Back, and G. Woltersdorf, Nat. Commun. **6**, 8274 (2015).
[21] G. van der Laan, J. Electron Spectros. Relat. Phenomena **220**, 137 (2017).
[22] M. Dabrowski, T. Nakano, D. M. Burn, A. Frisk, D. G. Newman, C. Klewe, Q. Li, M. Yang, P. Shafer, E. Arenholz, T. Hesjedal, G. van der Laan, Z. Q. Qiu, and R. J. Hicken, Phys. Rev. Lett. **124**, 217201 (2020).
[23] G. van der Laan, C. R. Physique **9**, 570 (2008).
[24] K. N. Stoev and K. Sakurai, Spectrochim. Acta, Part B At. Spectrosc. **54**, 41 (1999).
[25] S. Macke and E. Goering, J. Phys. Condens. Matter **26**, 363201 (2014).
[26] D. M. Burn, S. Zhang, K. Zhai, Y. Chai, Y. Sun, G. Van Der Laan, and T. Hesjedal, Nano Lett. **20**, 345 (2020).
[27] D. M. Burn, S. L. Zhang, G. Q. Yu, Y. Guang, H. J. Chen, X. P. Qiu, G. van der Laan, and T. Hesjedal, Phys. Rev. Lett. **125**, 137201 (2020).
[28] T. A. W. Beale, T. P. A. Hase, T. Iida, K. Endo, P. Steadman, A. R. Marshall, S. S. Dhesi, G. van der Laan, and P. D. Hatton, Rev. Sci. Instrum. **81**, 073904 (2010).
[29] C. A. Thomas, G. Rehm, H. L. Owen, N. G. Wyles, S. W. Botchway, V. Schlott, and M. Wahl, Nucl. Instruments Methods Phys. Res. Sect. A Accel. Spectrometers, Detect. Assoc. Equip. **566**, 762 (2006).
[30] W. Li, I. Bykova, S. Zhang, G. Yu, R. Tomasello, M. Carpentieri, Y. Liu, Y. Guang, J. Gräfe, M. Weigand, D. M. Burn, G. van der Laan, T. Hesjedal, Z. Yan, J. Feng, C. Wan, J. Wei, X. Wang, X. Zhang, H. Xu, C. Guo, H. Wei, G. Finocchio, X. Han, and G. Schütz, Adv. Mater. **31**, 1807683 (2019).
[31] S. Ishiwata, Y. Taguchi, and H. Murakawa, Science **319**, 1643 (2008).
[32] F. P. Chmiel, D. Prabhakaran, P. Steadman, J. Chen, R. Fan, R. D. Johnson, and P. G. Radaelli, Phys. Rev. B **100**, 104411 (2019).
[33] A. M. Mulders, S. M. Lawrence, A. J. Prncepi, U. Staub, Y. Bodenthin, M. García-Fernández, M. Garganourakis, J. Hester, R. MacQuart, and C. D. Ling, Phys. Rev. B **81**, 092405 (2010).